Final author version

Design, Realisation and Evaluation of a Liquid Hollow Torso Phantom Appropriate for Wearable Antenna Assessment

Aris Tsolis ; **Anastasios Paraskevopoulos** ; **Antonis Alexandridis** ; **William Whittow** ; **Alford Chauraya** ; **John Vardaxoglou**

Source: IET Microwaves, Antennas & Propagation, 17 pp.
DOI: 10.1049/iet-map.2016.0235

http://digital-library.theiet.org/content/journals/10.1049/iet-map.2016.0235

Design, Realisation and Evaluation of a Liquid Hollow Torso Phantom Appropriate for Wearable Antenna Assessment

Aris Tsolis[1,2], **Anastasios Paraskevopoulos**[1,2], **Antonis A. Alexandridis**[2], **William G. Whittow**[1], **Alford Chauraya**[1], **J(Yiannis) C. Vardaxoglou**[1]

[1]: School of Electronic, Electrical and Systems Engineering, Loughborough University, Loughborough, LE11 3TU, UK
[2]: Institute of Informatics & Telecommunications, National Centre for Scientific Research "Demokritos", Athens, 15310, GREECE

Abstract

This paper examines the design, realization and evaluation of a lightweight and low cost hollow oval cross-section torso phantom appropriate for wearable antenna performance assessment. The phantom consists of an empty inner space (hollow) surrounded by a shell with double plastic walls between which there is a tissue simulating liquid. The phantom's plastic shell is made of a low loss cast acrylic and the liquid is a commercially available one with properties calibrated for the frequency range of 2 - 6 GHz. The proposed phantom is compared, through simulations, with a full liquid torso phantom and a heterogeneous anthropomorphic voxel phantom. Additionally, the fabricated phantom is compared with human bodies and a homogeneous anthropomorphic solid phantom, through measurements. The phantom performance is tested in terms of electric field distribution of a wearable antenna on its surface and the path loss between two wearable antennas, on either side of the phantom. It is proved that the hollow phantom performance approximates the full liquid phantom when an RF absorbing material is placed in the central hollow region. The phantom performance in terms of S_{11} wearable antenna measurements is evaluated and found in good agreement with real human bodies in the examined frequency range (2 - 6 GHz). The far field wearable antenna performance of the proposed phantom shows deviation in gain less than 1.5 dB, compared with anthropomorphic phantom.

1. Introduction

Wearable antennas and electronics are meant by definition to be part of the garments or to be worn by humans. Smart garments with wearable antennas will emerge in various applications including: sports , emergency workers [1], search and rescue [2] military [3], medical [4], [5] and space [6] applications or even in casual clothes or fashion. A recent review of wearable antennas is presented in [7]. The importance of wearable antennas is that their use would exclude the implementation of bulky, not comfortable and non-low profile of conventional portable wearable communication systems, antennas and monitors that have been used so far.

Test and evaluation of antennas or electronic systems mounted on a person can be a really challenging procedure [8]. Due to ethics, safety and repeatability issues it is not appropriate to use a real person inside an anechoic chamber for wearable antennas performance evaluation. This requires the design, the realization and the use of an equivalent phantom which represents the human body shape and electrical properties. Hence, the use of phantoms for wearable antenna measurements can provide a stable and controllable propagation environment that cannot be easily realized with alive human subjects [9]. Such measurements exclude the dynamic nature of real human bodies and give an ideal and stable wearable antenna performance.

Phantoms can be categorized from several different points of view such as the frequency range, the type of tissues the phantom represents and the internal structure which can be a) liquid, b) semisolid (gel), or c) solid (dry) [9], [10]. The liquid phantom is a container filled with a liquid that simulates the electrical properties of the tissues of the body in a specific frequency range. Such phantoms have a thin shell usually made from fiberglass or plastic and it is preferred that the shell has a low relative permittivity (≤ 5), the loss tangent should be less than 0.05 and its thickness should be 2±0.2 mm in the frequency range of 0.8 to 3 GHz [11]. The shell has a shape of a human head or a whole body (depending on the requirements of the application) [9]. A simple square shaped liquid phantom has been already presented in [12] and a homogeneous anthropomorphic whole body liquid phantom is used for measurements in [13]. More examples of all the types of phantoms are extensively described in [5], [7], [9], [14],[15], [16], [17].

In this paper a liquid torso phantom with a hollow oval cross – section (HOCS) structure is designed, characterized and evaluated in terms of wearable antenna performance. The goal of HOCS phantom is to give similar or comparable wearable antenna performance with a respective full liquid, with real human bodies and anthropomorphic phantoms. A previous paper has briefly introduced the concept of the HOCS phantom via limited simulations and measurements only at the 5.8 GHz band [18]. Additionally, the designed HOCS phantom in [18] differs with the proposed and realized HOCS phantom in this paper, regarding the dimensions, the plastic shell dielectric properties and the liquid tissue simulating thickness. The realized HOCS is lighter than a full liquid phantom having a low fabrication cost. The procedure followed for the evaluation is proposed as a method for evaluating phantoms which are appropriate for wearable antenna measurements (reflection coefficient; near field; on-body communication link budget and far field).

The paper is outlined as: in Section 2 the hollow torso phantom is classified and compared with other liquid phantoms that have already been proposed and used. The dielectric and geometrical properties of HOCS phantom are described. In Section 3, the electric field distribution on, in and around the phantom is examined and compared with the full liquid phantom via simulations. Additionally, S_{11} measurements on the realized phantom and on different volunteers are presented and compared in order to study the validity of the phantom for such measurements. The simulated path loss (S_{21}) for on-body communication links on the HOCS phantom is compared with the results on the full liquid phantom. Finally, the far field

behavior of the proposed phantom is investigated and compared with other phantoms (full liquid and anthropomorphic), via simulations and measurements.

2. Phantom Geometry and materials

2.1 Geometry

The dimensions of the proposed phantom are shown in Fig. 1a. These dimensions approximate the average anthropomorphic phantom torso dimensions [19],[20]. The phantom has an oval cross-section geometry which has a more accurate shape to that of a real human torso compared with a cylindrical [21]. The idea for the structure of the phantom was derived from [22] where an oval cross-section phantom was proposed and successfully used for wearable antenna measurements. That phantom was fully filled with liquid. The proposed HOCS phantom will simplify the measurement setup compared with a heavier full liquid phantom. Note the HOCS phantom does not have arms, legs and head.

a)

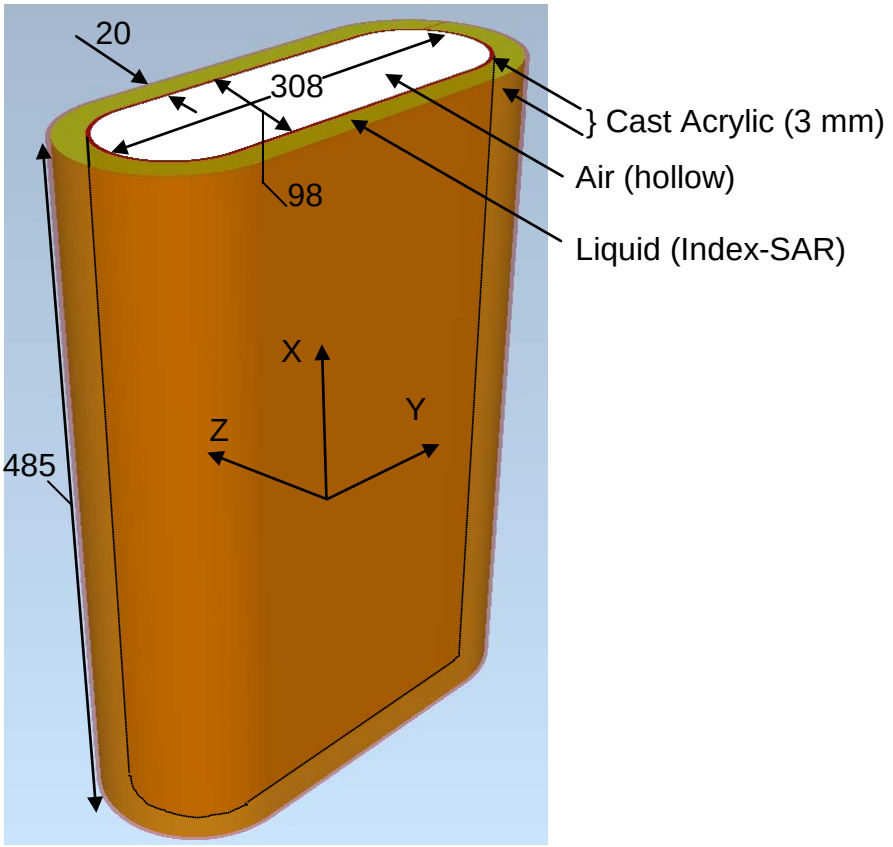

b)

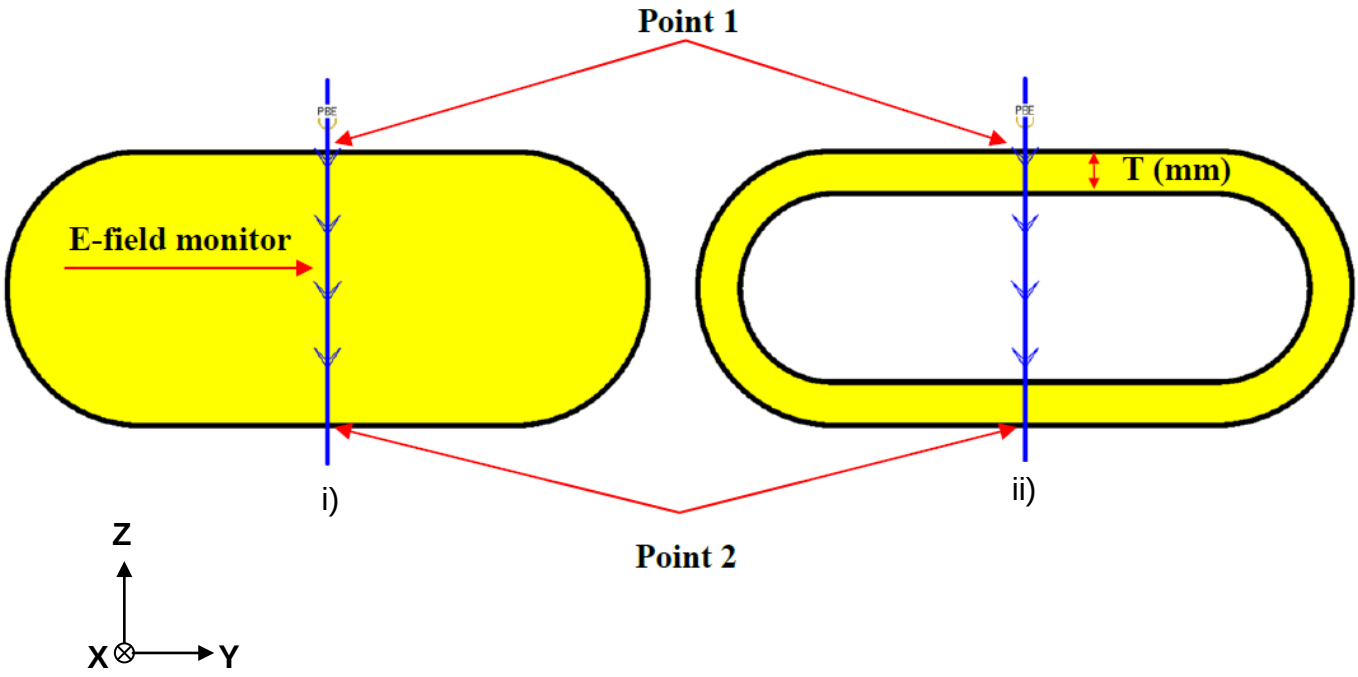

Fig. 1 a) 3D HOCS phantom geometry (dimensions in mm) and b) E-field line monitors simulation analysis model setup: i) full liquid and ii) HOCS with variable thickness

2.2 Phantom material properties

The HOCS phantom has two parts: a) the outer shell which is made from a low loss cast acrylic and b) the liquid simulating tissue. The dielectric properties of the liquid have the average human body values and have been characterized for the frequency range of 2 to 6 GHz and was produced by Index-SAR [20] (Table I). The liquid dielectric properties follow the standard: IEEE 1528-2013 [20]. Before the design and construction of the phantom, the dielectric properties of cast acrylic were measured by using three different split post dielectric resonators at 1.1; 1.9 and 2.4 GHz [23], [24]. These properties are listed in Table II and were used in simulations, in order to design and evaluate the phantom as described in the following sections. The properties of cast acrylic component for higher frequencies (e.g. 6 GHz) have been estimated by applying the linear least square fitting method.

TABLE I. GIVEN PROPERTIES OF LIQUID SIMULATING TISSUE PROPERTIES FROM INDEX-SAR

f_c (GHz)	ε_r	$tan\delta$	σ (S/m)
2.00	43.90	0.2681	1.31
2.45	42.47	0.3023	1.75
3.00	40.78	0.3452	2.35
4.00	37.53	0.3688	3.08
5.00	34.38	0.4402	4.21
5.80	31.95	0.5112	5.27
6.00	31.41	0.5125	5.32

TABLE II. MEASURED PROPERTIES OF THE PHANTOM SHELL MATERIAL (CAST ACRYLIC)

f_c (GHz)	ε_r	$tan\delta$	σ (S/m)
1.09	2.70	0.0075	0.0012
1.91	2.68	0.0076	0.0021
2.44	2.67	0.0076	0.0027

As can be seen from Table II cast acrylic (shell) is a low loss material and this property could characterize it as a good candidate to approximate garments [8], as long as the wearable antennas are generally mounted onto garments. However, the values of the permittivity are higher compared with garments [8]. This is easily understandable considering that cast acrylic is plastic and denser than woven, knitted etc. garments. Finally, the thickness of the cast acrylic was chosen to be equal to 3mm so as to provide good mechanical stability of the structure and is comparable with other phantoms (Table III). The dielectric properties and the dimensions of the shell (3 mm thickness) do not significantly affect the phantom influence on wearable antenna performance as it will be shown in the next sections. However and more specifically the phantom shell existence and its dielectric properties slightly affect the wearable antenna detuning (S_{11}) especially in the lower frequencies (close to 2GHz). This is explained in section 3.2. The shell existence does not highly affect any other antenna performance parameters, such as the E-field distribution, path loss (S_{21}) and far field because the high dielectric liquid in the phantom dominates the lower dielectric shell. Finally, the HOCS phantom construction has been undertaken in a specialized oven where an orthogonal piece of cast acrylic was manipulated to form the oval shape of the HOCS structure.

2.3 Hollow torso phantom comparison with other liquid phantoms

The HOCS phantom characteristics are compared with liquid phantoms proposed by other researchers in Table III. The parameters used to compare the liquid phantoms are: shape of the phantom, dielectric constant and thickness of the shell and the frequency where the referred phantoms were used for wearable antennas measurements.

TABLE III. HOCS TORSO PHANTOM COMPARISON WITH OTHER LIQUID PHANTOMS

Phantom shape	**Shell**		**Frequency** (GHz)	**Reference**
	ε_r	Thickness (mm)		
HOCS	2.70	3	1.09	TABLE II
Oval Cross Section	3.40	2	2.45	[22]
Cubic	2.10	5	0.90	[12]
Anthropomorphic (Mannequin)	2.00	3-8	0.30	[13]
Anthropomorphic (Multi Postural)	NA	3-5	0.90	[25]

3. Phantom Characterization and Evaluation

3.1 Simulated electric field distribution and attenuation on and in phantom

3.1.1 Attenuation in the phantom

In this subsection the effect of the liquid thickness on the electric field distribution has been analyzed. The aim was to reduce the liquid volume by at least 60% compared with the full liquid phantom which resulted into a reduction of the cost approximately by 2/3. It is described why the 20 mm liquid thickness (Fig. 1a) was selected instead of making the

phantom non-hollow (full liquid) or choosing another liquid thickness. A cylindrical dipole antenna of length equal to 62 mm was designed to operate at 2 GHz which is the largest wavelength [24], [26] that the liquid is calibrated for (Section-2.2). Hence, the attenuation of the field in the lower frequency is less compared to the higher frequencies. The dipole was placed 10mm from the body surface which is a common separation distance for a wearable antenna [27]. At this distance the dipole antenna suffers less dielectric loading and no frequency detuning from the phantom compared to the lower distances down to the 0mm distance. This simplifies the analysis followed in this section (E-field analysis) by excluding the parameter of frequency detuning effect (S_{11}-section 3.2). This antenna has electric field propagation normal to the phantom surface. The analysis was based on the simulation results of the electric field attenuation from the front side (where the antenna was mounted) to the back side of the phantom. The basic concept is that the electric field attenuation should be comparable with the results derived from the simulations with the full liquid phantom [22], which resulted into a field attenuation comparable with a real human body.

The simulation analysis was carried out in a Finite-Difference Time-Domain (FDTD) 3D electromagnetic field simulator (Empire-XPU [28]). An E-field simulator's monitor was used in order to observe the E-field attenuation (A) in the phantom for the case of full liquid and various liquid thicknesses of the HOCS phantom. The setup of the simulation models used for this analysis can be seen in Fig. 1b. Point 1 is the position on the front side of HOCS and point 2 is the position on the opposite surface. These points are marked in the electric field results to facilitate the comparison of the attenuation of the electric field for all the phantoms simulated.

The E-field attenuation in dB for all the liquid thickness cases and the full liquid case is shown in Table IV. The E-field attenuation is almost the same in full liquid and in HOCS phantom with liquid thicknesses greater than 45 mm. Hence, it can be derived that the liquid thickness 45 mm should be the best solution approximating the performance of the full liquid case. However, another criterion which led to the final choice for 20 mm liquid thickness is the liquid volume reduction of the hollow phantom compared with the full liquid phantom's volume. The aim of HOCS volume was set to be equal or less than 40% of the full liquid phantom volume. The percentage of the volume for each liquid thickness compared with the full liquid one is shown in Table IV as well.

TABLE IV. ELECTRIC FIELD ATTENUATION (DB) FROM POINT 1 TO 2 AT 2GHZ AND HOCS PHANTOM VOLUME COMPARISON WITH THE FULL LIQUID PHANTOM FOR VARIOUS LIQUID THICKNESSES

T (mm)	**V_{HOCS} / V_{FULL}**	**A(dB)**
15	26.59%	45.4
20	34.79%	55.6
25	42.64%	58.1
30	50.17%	62.6
35	57.35%	68.1
40	64.18%	70.9
45	70.70%	76.9
50	76.86%	77.1
55	82.71%	76.9
Full Liquid	100.00%	78.4

3.1.2. Absorber modification

Section 3.1.1 conclusion is for using a 20 mm liquid thickness hollow phantom. Additionally, another solution, proposed, is a modification in HOCS phantom. This modification has an RF absorbing material (ferrite tile with ε_r = 15 [29], simulated target absorption = 1 dB/mm) in the middle of HOCS, instead of being hollow. The simulated E-field attenuation in dB for the cases of HOCS, HOCS with absorber and the full liquid phantoms are shown in Fig. 2a. The E-field attenuation of HOCS with the absorbing material is closer to the full liquid compared with the HOCS without the absorbing material.

In order to give a full image of the effect of the absorber addition on the electric field distribution in and around the phantom compared with the full liquid and HOCS phantom versions, the 2 GHz dipole's (Section 3.1.1) E-field plane cuts were recorded. The dipole's polarization was vertical (X-axis) and horizontal (Y-axis). The XZ and YZ plane cuts electric field distribution are shown in Fig. 2b and 2c. In terms of the electric field distribution around the phantom, the addition of the absorber brings the HOCS phantom's performance closer to the full liquid phantom. Finally it must be clarified that the null close to the end of x-axis (Fig. 2a) for all phantoms examined means that strong standing waves are initiated at these points.

a)

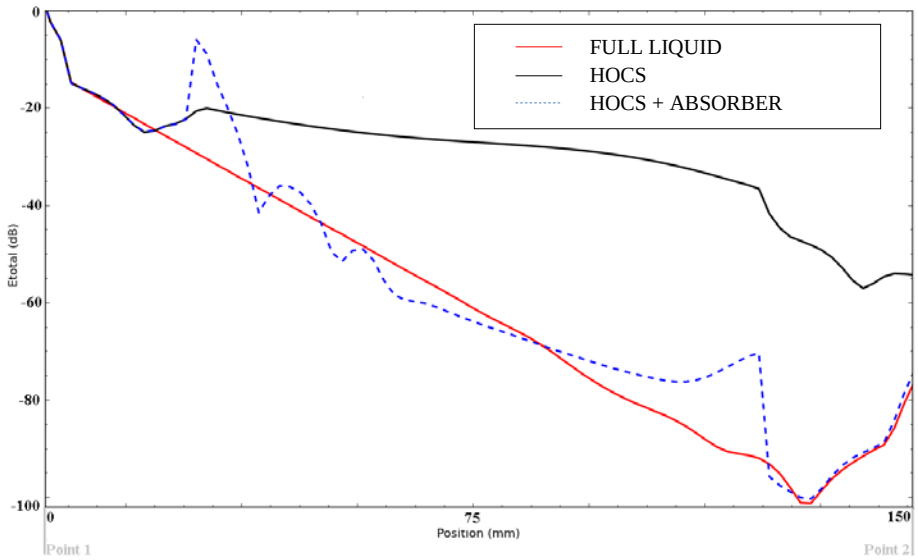

b)

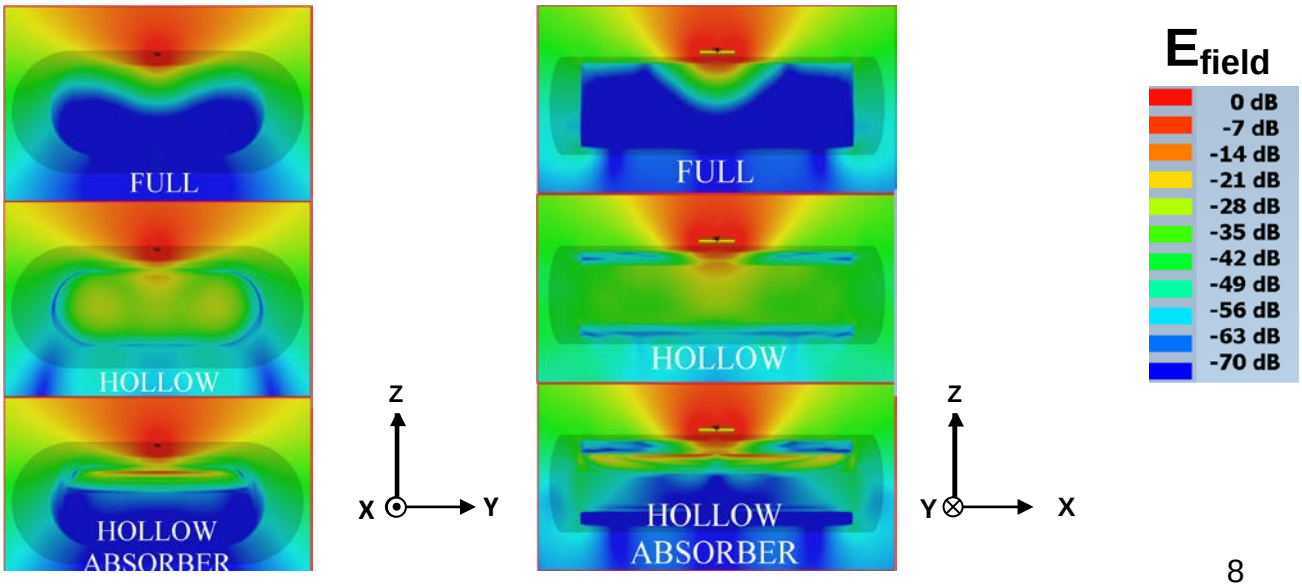

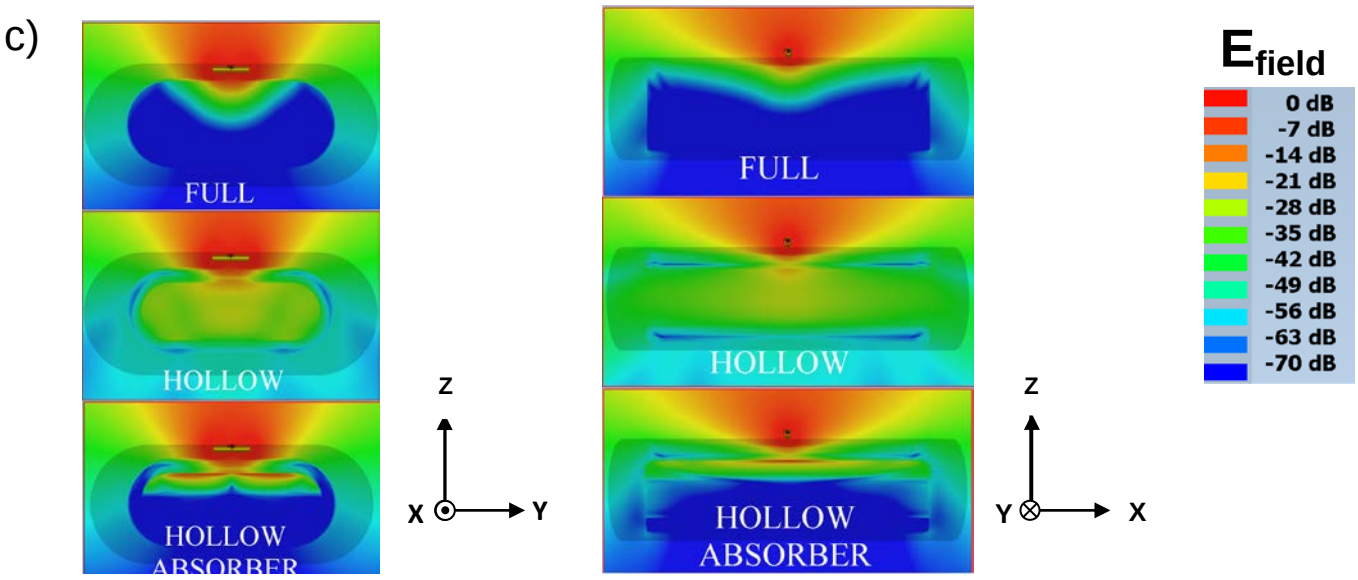

Fig. 2 a) Simulated E-field line monitor at 2GHz for the cases of: full liquid, HOCS and HOCS + absorber phantoms, b) and c) simulated YZ and XZ plane cuts of the E-field distribution of a: b) Vertical and c) Horizontal polarized dipole (2GHz) for: full, HOCS and HOCS + absorber phantoms

3.2 Phantom Influence on the Reflection Coefficient of a Wearable Antenna

The wearable antenna is dielectrically loaded by the human body tissues. Therefore, the antenna input impedance (Z_{in}) is affected by the body/phantom [9],[30]. So, it is important to evaluate the HOCS phantom for wearable antenna S_{11} measurements. Various S_{11} measurements were carried out on HOCS and compared with respective ones, obtained from three different volunteers (Fig. 3). For the S_{11} measurements three antennas were used: two sleeved balanced dipoles and a printed monopole antenna resonating at 2, 2.5 and 5.8 GHz respectively [26],[31]. The antennas were mounted directly against the plastic shell (HOCS) and the clothes (volunteers). The input impedance matching (S_{11}) of these kinds of antennas is highly affected by the presence of the human body/phantom. This is the reason why these antennas were selected for the wearable antenna reflection coefficient measurements evaluation of the phantom.

Fig.3 Measurements setup of the 2GHz sleeved balanced dipole antenna mounted on the middle of the torso of a volunteer and of the HOCS torso phantom

It can be noticed from Fig. 4a that the effect (downshift the resonant frequency of the dipole antenna) of the three different bodies (volunteers) is likewise to that of the HOCS

phantom. More specifically the frequency downshift of volunteers 2 and 3 is equal to 0.1 GHz whilst that of volunteer 1 is 0.2 GHz and finally HOCS phantom gives a downshift equal to 0.3 GHz. The S_{11} results deviation between HOCS phantom and human bodies is due to the value of the dielectric constant (Table I) of the phantom shell material (Cast Acrylic). To prove this a parameter sweep simulation analysis (for the 2GHz dipole antenna) for various values of the dielectric constant of the phantom shell was performed and the results are shown in Fig. 4d. It can be clearly seen that the value of the dielectric constant of the phantom shell affects the downshift of the resonant frequency. A phantom shell with a dielectric constant equal to 1.3 will give a better approximation.

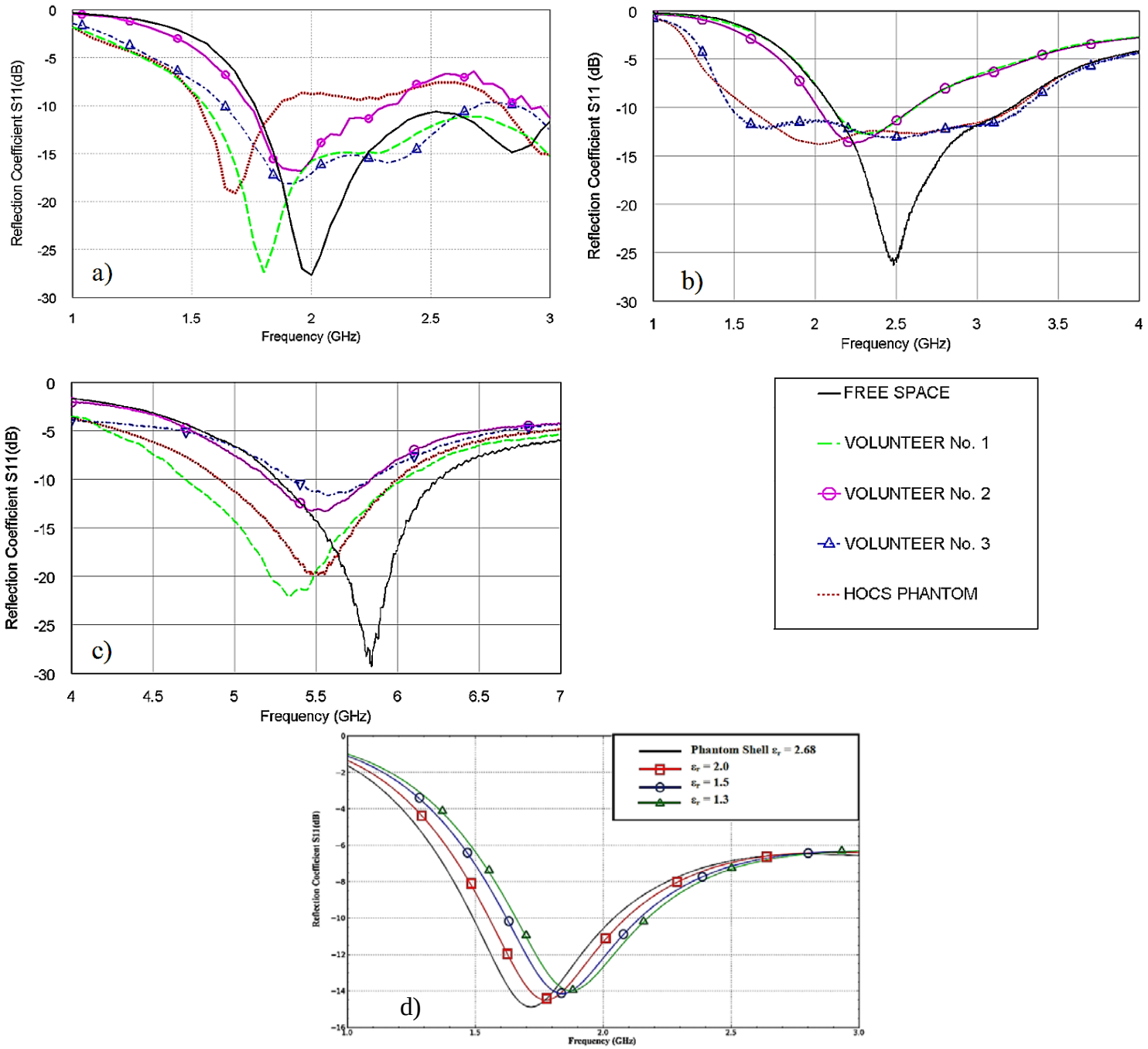

Fig. 4 a),b) and c) measured S11 of a sleeved balanced dipole antennas operating at: a) 2GHz and b) 2.5GHz and c) a printed monopole resonating at 5.8GHz in: Free Space, on three volunteers and on HOCS phantom and d) simulated S11 results of a sleeved balanced dipole antenna for various values of the dielectric constant of the shell of the phantom

S_{11} measurement results with the dipole (2.5 GHz) and the printed monopole (5.8 GHz) are shown in Fig.4b and Fig.4c respectively. Fig. 4b shows that HOCS phantom frequency downshift and detuning is within the respective downshift and detuning caused by the volunteers. It can be noticed from Fig. 4c that there is a good agreement between real human bodies and the HOCS phantom effect on the S_{11} at the high frequency range (5 – 6 GHz) that the liquid electrical properties are calibrated for.

As the liquid properties are calibrated for the frequency range 2 - 6 GHz the HOCS phantom performance presents better agreement with real human bodies for frequencies higher than the lower frequency limit (2 GHz). For a plastic shell with lower dielectric constant the phantom would give better agreement with real human bodies in terms of S_{11} at the lower liquid frequency limit of the 2 GHz band.

3.3 Phantom influence on path loss for On-body communication links

Wearable communication systems include the possibility of two communicating antennas. The signal transmission between two antennas, mounted on the phantom, was examined to evaluate the performance of the HOCS phantom under these conditions compared with the full liquid phantom and with the HOCS torso phantom filled with the absorbing material. The simulation scenario followed for this evaluation is illustrated in Fig. 5a. Two dipole antennas were mounted at a distance of 10 mm from the phantom surface on the front and the back side of the phantom respectively. The S_{21} was examined when both dipoles were vertically (X-axis) and horizontally (Y-axis) polarized. Three cases were examined: the full liquid, HOCS and HOCS with absorber phantoms. The S_{21} results for the three cases can be seen in Fig. 5b. It can be noticed from the presented simulation results that the addition of the absorbers reduces the S_{21} deviation between the two 2 GHz dipoles in the case of HOCS phantom. Similar simulations for dipoles resonating in higher frequencies (2.5; 3.5 and 5.5 GHz) were carried out, in order to examine the effect of HOCS and the addition of the absorber in higher frequencies. The S_{21} values for the higher frequency resonating dipoles for Vertical and Horizontal polarizations are shown in Table V. It can be seen that even for higher frequencies the use of the absorber is important to obtain S_{21} results similar to those of the full liquid phantom.

a)

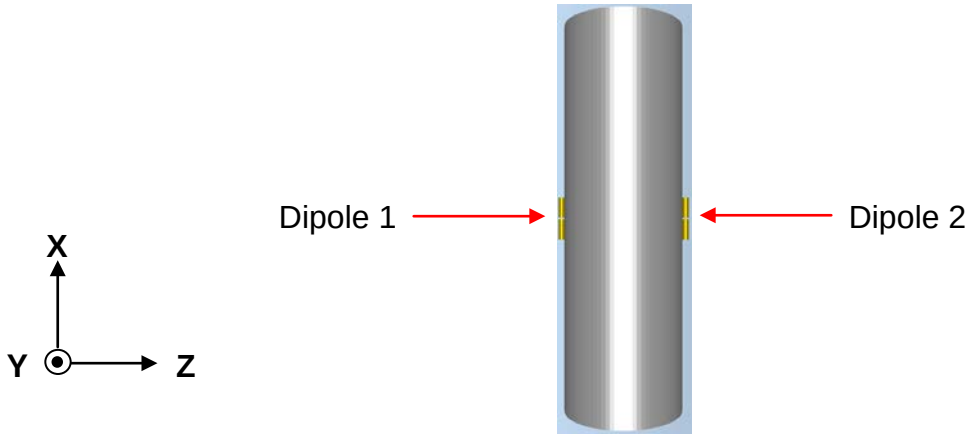

b)

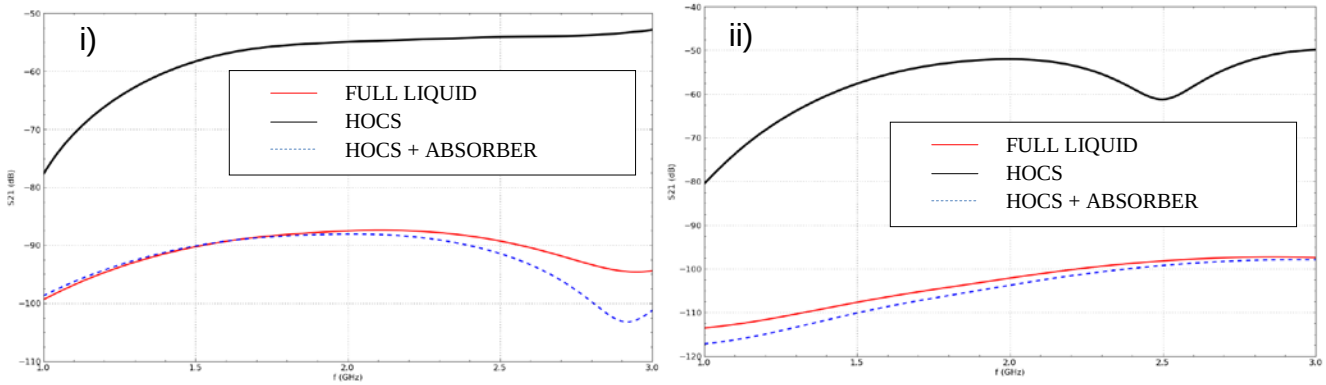

Fig. 5 Simulations: a) Model of two dipole antennas communicating on torso phantom and b) S_{21} results for dipoles resonating at 2GHz for full liquid, HOCS and HOCS + absorber phantoms: i) Vertical and ii) Horizontal polarization cases

TABLE V. PATH LOSS (S21) FOR FULL LIQUID, HOLLOW, HOLLOW WITH ABSORBER PHANTOMS: A) VERTICAL AND B) HORIZONTAL POLARIZATION CASES FOR DIPOLES RESONATING AT 2.5, 3.47 AND 5.5 GHZ

	Path loss - S_{21} (dB)					
Frequency (GHz)	**Vertical**			**Horizontal**		
	Full Liquid	*HOCS*	*HOCS + Absorber*	*Full Liquid*	*HOCS*	*HOCS + Absorber*
2.50	-94.5	-61.9	-94.6	-120.2	-63.4	-113.3
3.47	-117.1	-82.4	-117.1	-141.9	-82.4	-140.4
5.50	-123.2	-118.0	-123.1	-150.0	-135.4	-153.1

3.4 Far Field Evaluation

3.4.1 Simulations

For the purposes of far field evaluation of the HOCS phantom three printed monopole antennas operating at 2.5, 3.47, 5.5 GHz were designed and simulated. These antennas were selected because they are highly affected by the presence of the lossy phantom and they operate in the frequency range where the phantom is designed for (2 - 6 GHz). The far field results derived from HOCS phantom was compared with the full liquid phantom and heterogeneous voxel anthropomorphic, which is a very good representation of the real human body, phantom (Fig. 6a) in Tables VI.

a)

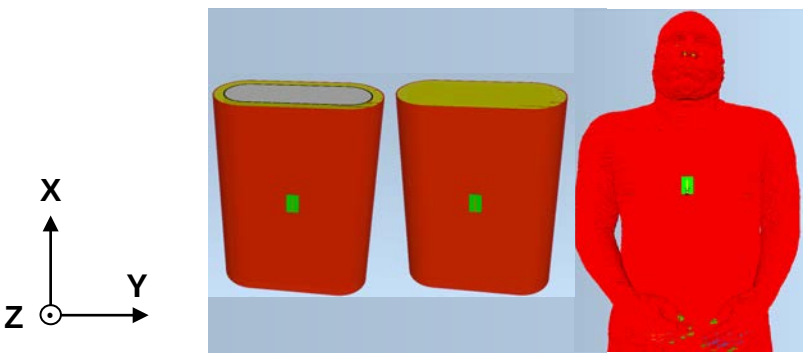

b)

Fig. 6 a) Simulation setups for far field evaluation: HOCS, Full Liquid and Voxel Phantom and b) Measurement setups for far field evaluation: Horizontal printed dipole antenna mounted on a HOCS and on a solid anthropomorphic torso phantom

TABLE VI. SIMULATED PARAMETERS OF PRINTED MONOPOLE ANTENNAS ON DIFFERENT TYPES OF PHANTOMS

2.5 GHz Printed Monopole Antenna				
Parameters	***Free Space***	***HOCS***	***Full Liquid***	***Voxel***
f_0 (GHz)	2.50	2.10	2.10	2.36
S11 (dB)	-21.8	-14.1	-14.4	-16.8
BW (GHz)	0.42	0.35	0.36	0.39
η_{rad} (%)	86.7	8.7	8.5	11.9
Gain (dBi)	+1.5	-3.8	-3.7	-2.0
FBR (dB)	-0.3	+24.1	+18.0	+31.7
3.47 GHz Printed Monopole Antenna				
Parameters	Free Space	HOCS	Full Liquid	Voxel
f0 (GHz)	3.47	3.10	3.10	3.33
S11 (dB)	-20.0	-12.3	-12.3	-15.0
BW (GHz)	0.735	0.48	0.48	0.64
ηrad (%)	85.3	14.9	15.0	16.4
Gain (dBi)	+1.7	-1.3	-1.3	-0.0
FBR (dB)	-0.9	+27.2	+23.2	+35.9
5.5 GHz Printed Monopole Antenna				
Parameters	Free Space	HOCS	Full Liquid	Voxel
f0 (GHz)	5.50	4.90	4.90	5.32
S11 (dB)	-30.7	-19.1	-19.1	-16.0
BW (GHz)	1.875	1.515	1.515	1.275
ηrad (%)	80.9	25.7	25.7	20.1
Gain (dBi)	+2.4	+1.7	+1.7	+1.2
FBR (dB)	-2.6	+33.1	+30.4	+35.9

The results showed that the HOCS and the full liquid phantoms are in a good agreement for the three antennas examined in terms of far field analysis (i.e. almost identical η_{rad} and Gain). Therefore the idea of removing part of the liquid and transforming the full liquid phantom into a hollow one is an effective and an acceptable phantom solution for far field performance estimation of a wearable antenna. The far field results of the HOCS phantom deviate from the corresponding results of the Voxel phantom. More specifically there is a deviation in terms of resonant frequency. There are small differences in terms of gain and efficiency. It can be seen from the front to back (FBR) ratio values that there is more energy absorbed at the backside of the Voxel phantom compared with the HOCS one. The

heterogeneity of the Voxel phantom increases the cross-polar components of the radiation patterns compared with those of the HOCS Phantom [18]. Taking into account the above simulation results, the proposed HOCS phantom is evaluated as an acceptable one for far field wearable antenna performance assessment compared with the respective full liquid phantom as a lighter and less expensive solution.

3.4.2 Measurements

In order to verify the simulated far field behavior of an antenna mounted on the HOCS phantom, corresponding measurements were carried out. These measurements used a printed dipole antenna mounted on the HOCS and on a homogeneous solid anthropomorphic phantom (Fig. 6b). This antenna was selected in order to verify the far field simulation behavior for the HOCS phantom for similar type of an antenna (dipole or monopole) and to examine the difference in the far field behavior between the HOCS and anthropomorphic phantoms. The selected antenna operates at the 2.4 GHz ISM-band and was measured for: vertical (X-axis) and horizontal (Y-axis) polarization orientation.

The normalized far field radiation patterns are shown in Fig. 7a for vertical polarization and in Fig. 7b for horizontal polarization. Additionally, the measured far field parameters (directivity, gain, radiation efficiency) are shown in Table VII. From the radiation patterns it can be said that generally there is an acceptable agreement between the realized HOCS phantom and the anthropomorphic torso phantom. Though, there are noticeable differences which need to be commented upon. More specifically in the case where the dipole is mounted vertically on the phantoms, the gain at the back side lobe is higher in the case of HOCS phantom. This means that the anthropomorphic phantom absorbs more power than HOCS. This is also noticed from the gain and efficiency values (Table VII). Additionally from Fig. 7a (Elevation plane), the co-polar results reveal the effect of the head presence in the case of the anthropomorphic phantom. In the angular range from 0^{o}-90^{o} the radiated gain is reduced in the case of the anthropomorphic phantom compared with HOCS phantom. Likewise results are noticed for the case of Horizontal polarization. Finally, the measured far field parameters (Table VII) present acceptable agreement for the directivity (maximum deviation equal to 0.2 dB) and for the Gain (maximum deviation of 1.2 dB). These correspond to a maximum deviation of 11% regarding the estimation of the wearable antenna radiation efficiency.

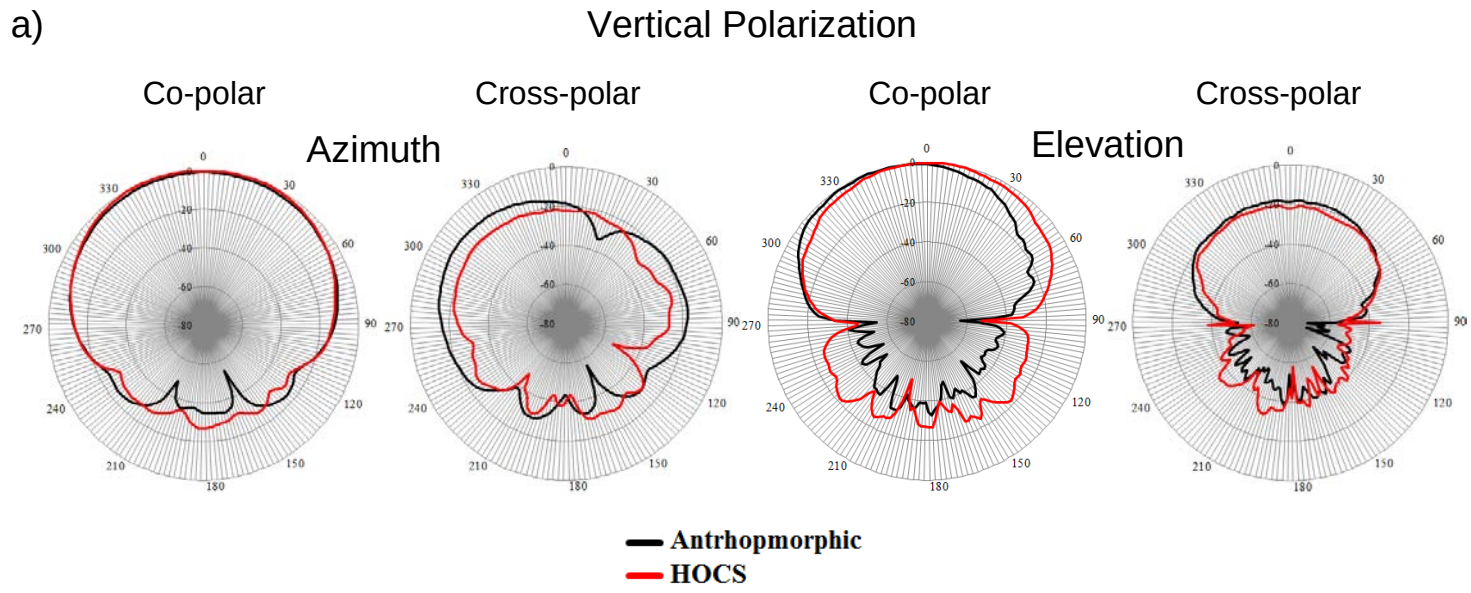

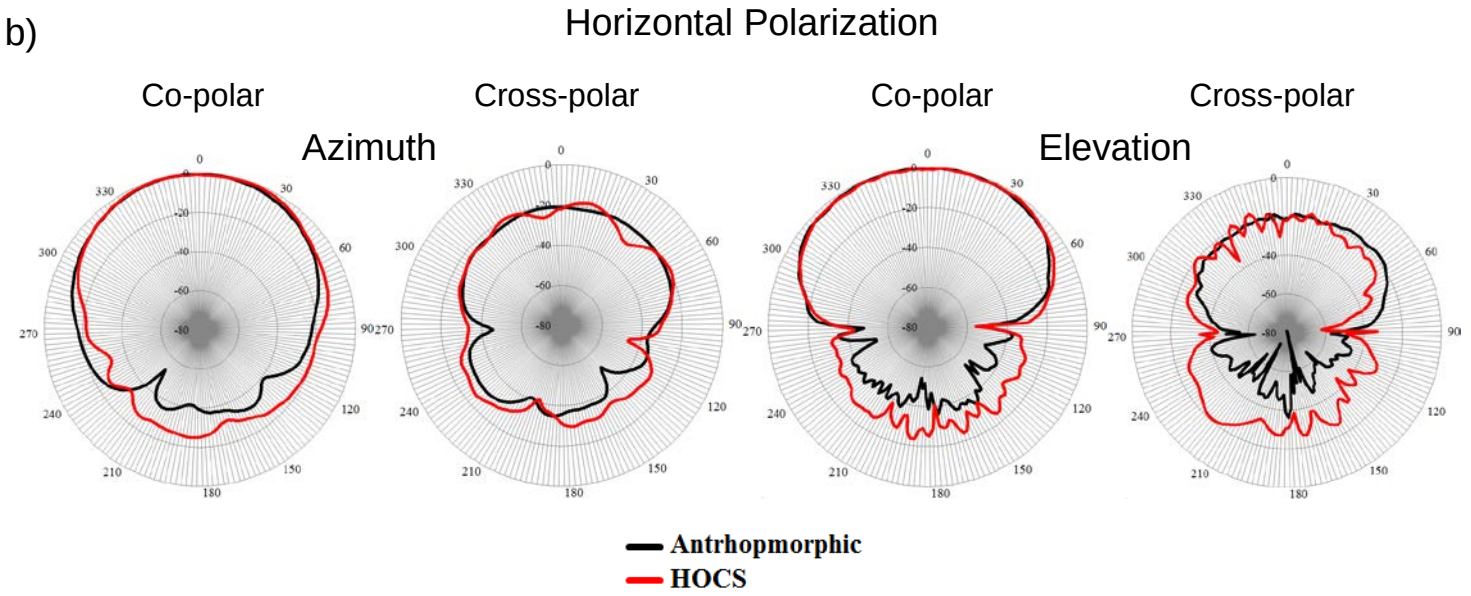

Fig. 7 Measured normalized radiation patterns of dipole antenna mounted with: a) Vertical and b) Horizontal polarization on HOCS (2.4GHz) and anthropomorphic (2.38GHz) phantoms on: Azimuth and Elevation planes

TABLE VII. MEASURED 2.4GHZ PRINTED DIPOLE ANTENNA FAR FIELD MEASURED PARAMETERS ON HOCS AND ON ANTHROPOMORPHIC PHANTOM

	HOCS phantom		***Anthropomorphic phantom***	
	Vertical	Horizontal	Vertical	Horizontal
f_c (GHz)	2.40		2.38	
S_{11} (dB)	-12.0		-14.6	
Directivity (dBi)	8.2	8.5	8.4	8.6
Gain (dBi)	4.3	4.5	3.0	3.7
η_{rad} (%)	40.4	40.2	29.4	36.4

4. Conclusions

This paper presents the design, realization and evaluation of a lightweight and a non-expensive hollow torso phantom appropriate for wearable antenna performance assessment. The main advantage of the proposed phantom is that its performance in terms of wearable antenna evaluation is comparable with full liquid, anthropomorphic phantoms and real human bodies. In terms of S_{11} wearable antenna performance HOCS phantom is in better agreement with real human bodies for frequencies higher than 2 GHz. In terms of electric field distribution or penetration, the HOCS phantom deviates from the full liquid. Additionally, the path loss performance, when considering two antennas either side of the HOCS phantom, differs from the full liquid one. The corresponding electric field distribution and path loss can be improved by using an RF absorbing material inside the inner empty space of HOCS phantom. In terms of far field wearable antenna performance, HOCS phantom results into small deviations (< 1.5 dB in Gain) compared with the corresponding simulation or measurement results on anthropomorphic phantoms. Finally, the proposed HOCS phantom is in very good agreement, regarding the far field wearable antenna performance, in comparison with the full liquid phantom.

REFERENCES

[1] Hertleer, C., Rogier, H., Vallozzi, L. and Van Langenhove, L.: 'A Textile Antenna for Off-Body Communication Integrated Into Protective Clothing for Firefighters', *IEEE Trans. Antennas Propag.*, 2009, **57**, (4), pp. 919–925.

[2] Seager, R.D., Chauraya, A., Vardaxoglou, J.C. and DeMaagt, P.: 'Towards a compact low frequency woven antenna', Proc. of the IEEE Antennas and Propagation Society International Symposium (APS-URSI), 2009, pp. 1–4.

[3] Psychoudakis, D., Lee, G., Chen, C. and Volakis, J.L.: 'Military UHF Body-Worn Antennas for Armored Vests', Proc. of the 4th European Conference on Antennas and Propagation (EuCAP), 2010, pp. 1–4.

[4] Zhang, L., Wang, Z., Salman, S. and Volakis, J.L.: 'Embroidered Textiles for RF Electronics and Medical Sensors', Proc. of the IEEE International Conference on Wireless Information Technology and Systems (ICWITS), 2012, pp. 1–4.

[5] Conway, G.A. and Scanlon, W.G.: 'Wearable antennas for medical monitoring systems', Proc.of the international Workshop on Antenna Technqology (iWAT), 2015, pp. 1051–1052.

[6] Kennedy, T.F., Fink, P.W., Chu, A.W., Champagne, N.J., Lin, G.Y. and Khayat, M.A.: 'Body-Worn E-Textile Antennas : The Good , the Low-Mass , and the Conformal', *IEEE Trans. Antennas Propag.*, 2009, **57**, (4), pp. 910–918.

[7] Wang, J.C., Lim, E.G., Leach, M., Wang, Z., Man, K.L. and Huang, Y.: 'Review of Wearable Antennas for WBAN Applications', *IAENG Int. J. Comput. Sci.*, 2016, pp. 16–19.

[8] Tsolis, A., Whittow, W.G., Alexandridis, A.A. and Vardaxoglou, J.C.: 'Embroidery and Related Manufacturing Techniques for Wearable Antennas: Challenges and Opportunities', *Electronics*, 2014, **3**, (2), pp. 314–338.

[9] Hall, P.S. and Hao, Y.: 'Antennas and Propagation for Body-Centric Wireless Communications' (Artech House, 2012, 2nd edn.)

[10] Tamura, H., Ishikawa, Y., Kobayashi, T. and Nojima, T.: 'A dry phantom material composed of ceramic and graphite powder', *IEEE Trans. Electromagn. Compat.*, 1997, **39**, (2), pp. 132–137.

[11] Kanda, M.Y., Ballen, M., Salins, S., Chou, C.K. and Balzano, Q.: 'Formulation and Characterization of Tissue Equivalent Liquids Used for RF Densitometry and Dosimetry Measurements', *IEEE Trans. Microw. Theory Tech.*, 2004, **52**, (8), pp. 2046–2056.

[12] Marrocco, G.: 'RFID Antennas for the UHF Remote Monitoring of Human Subjects', *IEEE Trans. Antennas Propag.*, 2007, **55**, (6), pp. 1862–1870

[13] Psychoudakis, D., Chen, C. and Volakis, J.L. 'Wearable UHF Antenna for Squad Area Networks (SAN)', Proc. of the IEEE Antennas and Propagation Society International Symposium (APS-URSI), 2008, pp. 1–4.

[14] Ogawa, K.: 'Electromagnetic human phantoms for the purpose of antenna design', Proc. of the international Workshop on Antenna Technology (iWAT), 2011, **2**, pp. 190–193.

[15] Guy, W.A.: 'Analyses of Electromagnetic Fields Induced in Biological Tissues by Thermographic Studies on Equivalent Phantom Models', *IEEE Trans. Microw. Theory Tech.*, 1971, **19**, (2), pp. 205–214.

[16] Ito, K.: 'Human Body Phantoms for Evaluation of Wearable and Implantable Antennas', Proc. of the 2nd European Conference on Antennas and Propagation (EuCAP), 2007, pp. 1–6.

[17] Loader, B. and Loh, T.H.: 'Phantoms for Antenna Measurements At 2.4 GHz', Proc.of the 6th European Conference on Antennas and Propagation (EuCAP), 2011, pp. 2285–2288.

[18] Tsolis, A., Whittow, W.G., Alexandridis, A.A. and Vardaxoglou, J.C.: 'Evaluation of a Human Body Phantom for Wearable Antenna Measurements at the 5 . 8GHz Band', Proc. of the Loughborough Antennas & Propagation Conference, 11-12 November, Loughborough, UK, 2013, pp. 414–419.

[19] SPEAG, "EM-Phantom User Manual V 4 . 3. 2015.", found in "http://www.speag.com/, accessed December 2016.

[20] "https://indexsar.com/product-category/phantoms/tissue-simulant-fluids-phantoms/fluids-tissue-simulant-fluids-phantoms/.", accessed December 2016 .

[21] "ETSI, technical report: Electromagnetic compatibility and Radio spectrum Matters (ERM); Improvement of radiated methods of measurement (using test sites) and evaluation of the corresponding measurement uncertainties ; Part 7 : Artificial human beings," 1998.

[22] Conway, G.A. and Scanlon, W.G.: 'Antennas for Over-Body-Surface Communication at 2.45GHz', *IEEE Trans. Antennas Propag.*, 2009, **57**, (4), pp. 844–855.

[23] Krupka, J., Geyer, R.G., Baker, J. and Ceremuga, J.: 'Measurements of the Complex Permittivity of Microwave Circuit Board Substrates Using Split Dielectric Resonator and Reentrant Cavity Techniques', Proc. of the Seventh International Conference on Dielectric Materials Measurements & Applications, 23-26 September, 1996, (430), pp. 21–24.

[24] Balanis, C.A.: 'Advanced Engineering Electromagnetics' (John Wiley & Sons, 2012 2nd edn.).

[25] Ogawa, K., Matsuyoshi, T., Iwai, H. and Hatakenaka, N.: 'A High-Precision Real Human Phantom for EM Evaluation of Handheld Terminals in a Talk Situation', Proc. of the IEEE Antennas Propag. Soc. Int. Symp., 2001, **2**, pp. 68–71.

[26] Balanis, C.A.: 'Antenna Theory Analysis and Design', (John Wiley & Sons, 2005, 3rd edn.).

[27] Paraskevopoulos, A., Alexandridis, A.A., Lazarakis, F. and Vardaxoglou, J.C.: 'Modelling of Dynamic On-Body Waist-Foot Channel', Proc. of the Loughborough Antennas & Propagation Conference (LAPC), 2013, pp. 155–160.

[28] "http://www.empire.de/media/pdf/Manual/EMPIRE-Manual-750.pdf.", accessed December 2016.

[29] "http://www.ets-lindgren.com/EMCAbsorbers.", accessed December 2016.

[30] Parini, C., Gregson, S., Mccormick, J. and Janse van Rensburg, D.: 'Theory and Practice of Modern

Antenna Range Measurements' (IET, 2015, 1st edn.).

[31] Balanis, C.A.: 'Modern Antenna Handbook' (John Wiley & Sons, 2008, 1st edn.).